NeuroImage: Clinical 28 (2020) 102462

Contents lists available at ScienceDirect

NeuroImage: Clinical

journal homepage: www.elsevier.com/locate/ynicl

Multi-channel hierarchy functional integration analysis between large-scale brain networks for migraine: An fMRI study

Yuhu Shi [a,*], Weiming Zeng [a], Weifang Nie [a], Jiajun Yang [b]

[a] College of Information Engineering, Shanghai Maritime University, Shanghai, China
[b] Department of Neurology, Shanghai Sixth People's Hospital East Affiliated to Shanghai University of Medicine & Health Science, Shanghai 201306, China

ARTICLE INFO

Keywords:
fMRI
Group independent component analysis
Brain networks
Dynamic functional connectivity
Graph analysis

ABSTRACT

Migraine is a chronic dysfunction characterized by recurrent pain, but its pathogenesis is still unclear. As a result, more and more methods have been focused on the study of migraine in recent years, including functional magnetic resonance imaging (fMRI), which is a mainstream technique for exploring the neural mechanisms of migraine. In this paper, we systematically investigated the fMRI functional connectivities (FCs) between large-scale brain networks in migraine patients from the perspective of multi-channel hierarchy, including static and dynamic FCs of group and individual levels, where the brain networks were obtained using group independent component analysis. Meanwhile, the corresponding topology properties of static and dynamic FCs networks in migraine patients were statistically compared with those in healthy controls. Furthermore, a graph metrics based method was used to detect the potential brain functional connectivity states in dynamic FCs at individual and group levels, and the corresponding topology properties and specificity of these brain functional connectivity states in migraine patients were explored compared with these in healthy controls. The results showed that the dynamic FCs and corresponding global topology properties among nine large-scale brain networks involved in this study have significant differences between migraine patients and healthy controls, while local topological properties and dynamic fluctuations were easily affected by window-widths. Moreover, the implicit dynamic functional connectivity patterns in migraine patients presented specificity and consistency under different window-widths, which suggested that the dynamic changes in FCs and topology structure between them played a key role in the brain functional activity of migraine. Therefore, it may be provided a new perspective for the clinical diagnosis of migraine.

1. Introduction

As an idiopathic headache disorder, migraine is characterized by moderate to severe pain, which consists of unilateral and pulsating headache attacks that are typically aggravated by physical activity (May, 2009). It is a common recurrent neurological disorder combining nausea, vomiting, and hypersensitivities to visual, auditory, olfactory and somatosensory stimuli (Schwedt et al., 2015), and is also a complex and subjective experience that includes sensory-discriminative, affective and cognitive aspects. Migraine headaches cause significant individual and societal burdens as a result of pain, such as environmental sensitivity, disability and even lost productivity (Schwedt and Dodick, 2009). Therefore, it is very important to explore the neural mechanism of migraine and form some available biomarker identification for the clinical diagnosis of migraine.

Numerous neuroimaging studies have shown structure and functional alterations in widespread brain regions of patients with migraine (Moulton et al., 2011; Eck et al., 2011; Maleki et al., 2012; Schwedt et al., 2014), such as the anterior cingulate cortex, orbitofrontal cortex, insula, temporal gyrus, posterior cingulate cortex, supplementary motor area, cerebellum and thalamus etc. Among them, resting-state functional magnetic resonance imaging (fMRI) is a noninvasive imaging technique which measures spontaneous brain activity as low frequency fluctuations in blood oxygen level-dependent signals (Fox and Raichle, 2007). During the resting state, correlated spontaneous fluctuations occur within spatially distinct and functionally related groups of cortical and subcortical regions, consisting of the human brain's intrinsic functional networks (Seeley et al., 2009). It has been used extensively to reveal the intrinsic typical and atypical functional architecture of the brain (Greicius, 2008). The changed features during the resting state

* Corresponding author.
E-mail address: shiyuhu@shmtu.edu.cn (Y. Shi).

https://doi.org/10.1016/j.nicl.2020.102462
Received 22 May 2020; Received in revised form 26 September 2020; Accepted 1 October 2020
Available online 8 October 2020

may serve as a marker to reflect the progress of multiple diseases, such as schizophrenia (Lui et al., 2009), Alzheimer's disease (Greicius et al., 2004), and Parkinson's disease (Wu et al., 2009).

In the past decade, the resting-state fMRI has been used to investigate the pathophysiology mechanism of migraine and to identify many dysfunctional brain areas, especially for delineating the neural underpinnings of the pain experience in migraine patients, such as the periaqueductal grey, anterior cingulate cortex (ACC), insular cortex and temporal lobe, which are mainly associated with pain processing and pain modulation (Moulton et al., 2011; Schwedt et al., 2015; Maleki and Gollub, 2016). For example, the primary somatosensory cortex (S1), secondary somatosensory cortex (S2), and the motor and premotor cortex (PMC) are proposed as constituting parts of the pain intensity and spatial discrimination pathway (Oshiro et al., 2009). Moreover, the ACC, the motor areas, the PMC and the supplementary motor area (SMA) form a module that contributes to response selection and the generation of sensory information (Cavina-Pratesi et al., 2006). Furthermore, the S1, S2, primary motor cortex (M1), secondary motor cortex (M2) and insular cortex are in the trigeminovascular pathway and have been implicated in the ascending trigemino- thalamo-cortical nociceptive pathway (Burstein et al., 2015). Previous studies have demonstrated that the S1, S2, PMC, M1 and SMA comprise the sensorimotor network (De Luca et al., 2005). In addition, an increasing body of literatures has shown that people with migraine have alterations in the functional connectivities (FCs) of regions which important for mediating sensory, affective, and cognitive components of pain (Smith et al., 2009; Russo et al., 2012a, 2012b; Schwedt et al., 2013; Mathur et al., 2015).

In 2011, Raichle et al. found that there were multiple independent, spatially coherent resting-state functional networks in the brain, including default mode network, sensorimotor network, dorsal attention network, executive control network, salience network, and frontoparietal network, etc. (Raichle, 2011), which have been confirmed by domestic and foreign scholars. In recent years, more and more researches reported that resting-state brain functional networks were directly related to pain processing, and found that these brain functional networks were abnormal in migraine patients (Mainero et al., 2011; Jin et al., 2013; Tessitore et al., 2015). For example, Mickleborough et al. used fMRI to assess the attentional control networks during visual spatial-orienting tasks in migraine patients as compared to non-migraine controls, and migraine patients showed less activation than non-migraine controls in a key area of the ventral frontoparietal network of attention (Mickleborough et al., 2016). Zhang et al. evaluated the dysfunction of the sensorimotor network in migraine patients and investigated whether the dysfunctional areas within the sensorimotor network exhibited abnormal FC with other brain areas based on resting-state fMRI (Zhang et al., 2017). Tessitore et al. demonstrated disrupted default mode network (DMN) connectivity in migraine and also showed decreased connectivity in prefrontal and temporal regions of the DMN (Tessitore et al., 2013). Tedeschi used voxel-based morphometry and diffusion tensor imaging to investigate the resting-state visual network integrity, and showed that patients with migraine had a significant increased functional connectivity in the right lingual gyrus within the resting-state visual network (Tedeschi et al., 2016). Russo et al. showed that migraine patients had significant functional connectivity reduction within the right frontoparietal network known to be associated with executive functions and specifically in the middle frontal gyrus and the dorsal anterior cingulate cortex (Russo et al., 2012a, 2012b).

However, to our knowledge, few studies has determined whether the symptoms of migraine are associated with functional connectivity and topological structure between these brain functional networks (BFNs), and the significance of altered resting-state brain functional connectivity in migraine is still unknown. The purpose of this study is to explore the differences of FCs and topological properties among multiple large-scale BFNs in migraine patients compared with health controls from the perspective of multi-channel hierarchy. Group independent component analysis (GICA) is used to obtain BFNs, and then explore the static FCs (SFCs) and dynamic FCs (SFCs) among these BFNs through sliding time-window correlation analysis at group and individual levels. Subsequently, complex network analysis is used to study the graph metrics of SFCs and DFCs, and a new graph metric based method is adopted to explore the dynamic pattern of change implicit in DFCs. The results showed the differences of FCs and topological structure among BFNs between migraine patients and healthy controls, which provided an important reference for the study of neurological pathogenesis and clinical diagnosis of migraine.

2. Materials and methods

2.1. Data acquisition

In this study, 48 migraine patients participated in the experiment came from the department of neurology of a hospital using the SIEMENS magnetic resonance instrument (3 T), which will be denoted as MPs in the following. All MPs were diagnosed with episodic or chronic migraine according to the diagnostic criteria set forth by the International Classification of Headache Disorders 3rd edition (beta version) (Headache Classification Committee of the International Headache Society, 2013). All the participants were informed consent before the data acquisition. In the process of data acquisition, all subjects were instructed to keep awake without think anything. The images dataset was acquired using single-shot SENSE gradient an echo planar imaging (EPI) with 38 slices, providing whole-brain coverage and 160 volumes, a repetition time (TR) of 3 s, and a scan resolution of 64×64. The in-plane resolution was 4 mm $\times$ 4 mm, and the slice thickness was 4 mm. The resting-state fMRI data of 49 healthy controls (HCs) were downloading from the public neuroimaging database (http://www.nitrc.org/projects/fcon1000/), which were used for the purpose of comparison. The image dataset was acquired using single-shot SENSE gradient echo EPI with 33 slices, providing whole-brain coverage and 225 volumes, a TR of 2 s, and a scan resolution of 64×64. The in-plane resolution was 3.13 mm $\times$ 3.13 mm, and the slice thickness was 3.6 mm.

2.2. Data preprocessing

In the experiment, all of the fMRI data were preprocessed by using the DPARSF software (http://rfmri.org/DPARSF), the first 10 time points of each fMRI data were discarded, and the other preprocessing steps included slice timing, motion correction, spatial normalization and spatial smoothing. Next, the sinc interpolation method and six degrees transformation method were applied to eliminate the time offset and spatial offset, respectively. In order to further minimize artifacts, the data which detected any direction of displacement is more than 1.5 mm or head rotation angle is greater than 1.5 degrees would be abandoned. When the head motion correction was completed, all data were normalized with echo planar imaging template released by Montreal neurological research institute. Finally, Gaussian kernel of 4 mm was taken to smooth all the data in order to make increase the signal to noise ratio of the data. Furthermore, the location and display of brain functional networks were assessed by using the MRIcro software (http://www.mricro.com).

2.3. Group independent component analysis

After preprocessing the data, the fMRI data of both MPs and HCs were analyzed by spatial GICA implemented in the GIFT software (https://trendscenter.org/software/) (Calhoun et al., 2001). Spatial ICA decomposes the subject data into linear mixtures of spatially independent components with a unique time course. Particularly, spatial ICA was implemented using FastICA algorithm (Shi et al., 2018) in the experiment, and minimum description length (Li et al., 2007) was used to estimate the number of independent components (ICs). To ensure stability of estimation, we repeated the ICA algorithm 20 times in ICASSO

(Himberg et al., 2004), and aggregate spatial maps were estimated as the modes of component clusters. Subject specific spatial maps and time courses were obtained using the spatiotemporal dual-regression back reconstruction approach implemented in GIFT software. In this study, we selected nine BFNs corresponding to ICs from GICA decomposition as the research objects.

2.4. Static and dynamic functional connectivity analysis

In this study, both SFCs and DFCs between large-scale BFNs were performed for MPs and HCs at group and individual levels, respectively. Among them, SFCs were obtained by Pearson correlation, whether between group BFNs or individual BFNs, and then the differences of SFCs between MPs and HCs were calculated. In particular, the difference at group level was measured on the overall FCs among the group BFNs, while the difference at individual level was measured on each pair of FCs between BFNs of all subjects. At the same time, the sliding time window correlation was used to obtain the DFCs among the BFNs at group and individual levels, in which the window width of 40 s for both MPs and HCs, window-widths of 60 s and 40 s for MPs and HCs separately, as well as window-width of 60 s for both MPs and HCs were used in this study. The differences of DFCs between each pair of BFNs and their overall variances between MPs and HCs were measured at group level, while the differences of mean DFCs and their variances corresponding to each pair of BFNs of all subjects between MPs and HCs were measured at individual level.

2.5. Dynamic functional connectivity states identification

Since this study focused on dynamic brain functional connectivity at both group and individual levels, a new method was used to detect DFC states at individual and group levels based on the metric of connectivity strength (Yu et al., 2015), which was different from the previous researches. First, the DFC states at individual level were obtained for each subject of MPs and HCs, which might reveal connectivity patterns reoccurring over subjects. For each graph of DFCs obtained from section 2.6, the connectivity strength of each BFN was computed by summing the FC strengths that it connected with other BFNs, and then got a connectivity strength matrix with a size of ($N \times W$) for each subject, in which N denoted the number of BFNs and W denoted the number of windows. In our study, the value of N was 9 for both MPs and HCs, and taking the situation of window-widths of 60 s and 40 s for MPs and HCs separately as example in the following, the value of W was 131 and 196 for MPs and HCs respectively.

In order to estimate how the brain connectivity patterns of different time- windows were associated to each other, a new similarity matrix with a size of ($W \times W$) was then computed based on correlations between each pair of columns of the connectivity strength matrix. Because modules of the similarity matrix may correspond to sets of time-windows with similar brain connectivity patterns, the modular organization of this similarity matrix was analyzed with the modularity algorithm of (Newman, 2006) implemented in the brain connectivity toolbox, and the number of modules was the number of connectivity states in this subject. Finally, the DFC graph of the time-windows which belong to the same module were averaged into one graph with a size of ($N \times N$), which was the corresponding connectivity state. A total of 261 connectivity states were identified for all subjects in both MPs and HCs (a range of 2 to 4 states per subject, totally 137 states in 48 MPs and 124 states in 49 HCs for this window-width situation).

Next, the DFC states at group level were obtained by grouping the connectivity states at individual level that showing related connectivity patterns, which might reveal connectivity patterns reoccurring over subjects. Similar to the individual level, the connectivity strength of each BFN in each connectivity state at individual level was computed by summing the FC strengths that it connected with other BFNs, and then got a connectivity strength matrix with a size of ($N \times E$), in which N denoted the number of BFNs and E denoted the number of connectivity states at individual level ($E = 137$ for MPs and $E = 124$ for HCs as well as $E = 261$ for both two groups). Then a new similarity matrix with a size of ($E \times E$) was computed based on correlations between each pair of columns of connectivity strength matrix. Following that, the modular organization of this similarity matrix was assessed. Finally, the graphs of connectivity states at individual level belonging to the same module were averaged into one graph, which was the corresponding connectivity state at group level. Two connectivity states were identified for MPs, HCs as well as both MPs&HCs in this window-width situation.

2.6. Graph theory analysis

Complex network is an analysis technology which developed based on graph theory, and using complex network theory to characterize the topological structure of brain functional or structural connectivity has gradually become an effective means of brain science research (Rubinov and Sporns, 2010). Therefore, we further study and analyze the topological properties of SFCs and DFCs of MPs and HCs using the complex network analysis method on the basis of functional connectivity analysis. Among them, the graph metrics included in this study are given as follows.

(1) Degree: the degree of a node refers to the number of edges directly connected to the node.
(2) Density: is the ratio of the number of directly connected edges to the number of possible connected edges.
(3) Assortativity coefficient (AC): is a correlation coefficient between the degrees of all nodes on two opposite ends of a link, and a positive AC indicates that nodes tend to link to other nodes with the same or similar degree.
(4) Local clustering coefficient (LCC) and global clustering coefficient (GCC): LCC is the fraction of triangles around a node and is equivalent to the fraction of node's neighbors that are neighbors of each other, and GCC is the average of LCC.
(5) Transitivity: is the ratio of triangles to triplets in the network and is an alternative to the clustering coefficient.
(6) Maximized modularity (MM): is a statistic that quantifies the degree to which the network may be subdivided into such clearly delineated groups.
(7) Optimal community structure (OCS): is a subdivision of the network into non-overlapping groups of nodes in a way that maximizes the number of within-group edges, and minimizes the number of between-group edges.
(8) Characteristic path length (CPL): is the average of the shortest path length between all nodes in the network and other nodes, where shortest path length is expressed by the minimum number of edges connected to two nodes.
(9) Global efficiency (GE) and local efficiency (LE): GE is the average inverse shortest path length in the network, and LE is the global efficiency computed on node neighborhoods.
(10) Small world (SW): SW network is a network model between regular network and random network, and it has the characteristics of high clustering coefficient of regular network and short shortest path length of random network.
(11) Betweenness centrality (BC): nodes with high values of BC participate in a large number of shortest paths.

2.7. Statistical analyses

Two-sample T-test and Wilcoxon Rank sum test were performed to test for group differences between MPs and HCs in the FCs strength and graph metrics as well as their dynamic variances. Specifically, the two-sample T-test with a confidence level of 95% was used to make a statistical comparison of SFCs and DFCs strengths as well as their corresponding graph metrics between MPs and HCs. Meanwhile, the

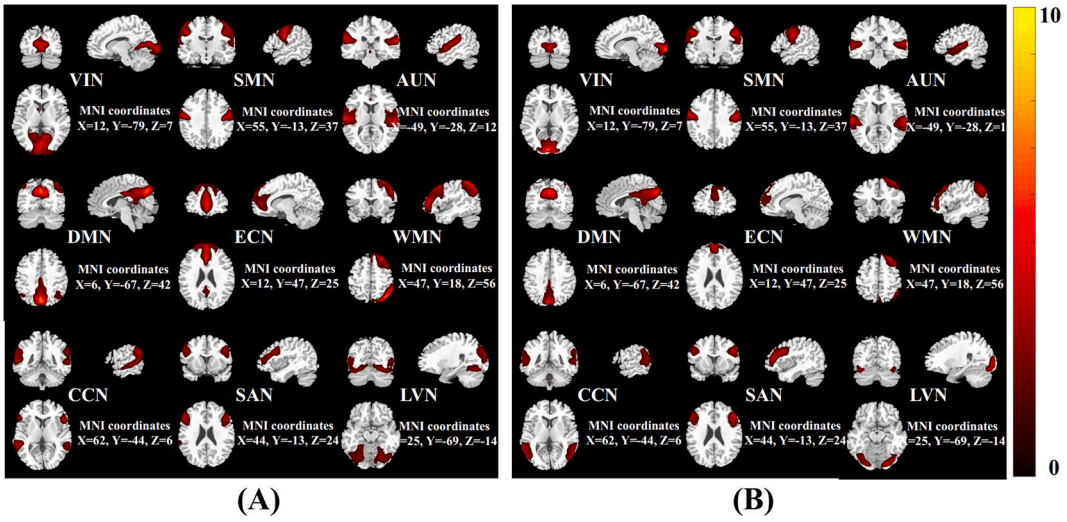

Fig. 1. the nine resting-state BFNs including VIN, SMN, AUN, DMN, ECN, WMN, CCN, SAN and LVN as well as their corresponding MNI coordinates, in which (A) represents HCs and (B) represents MPs.

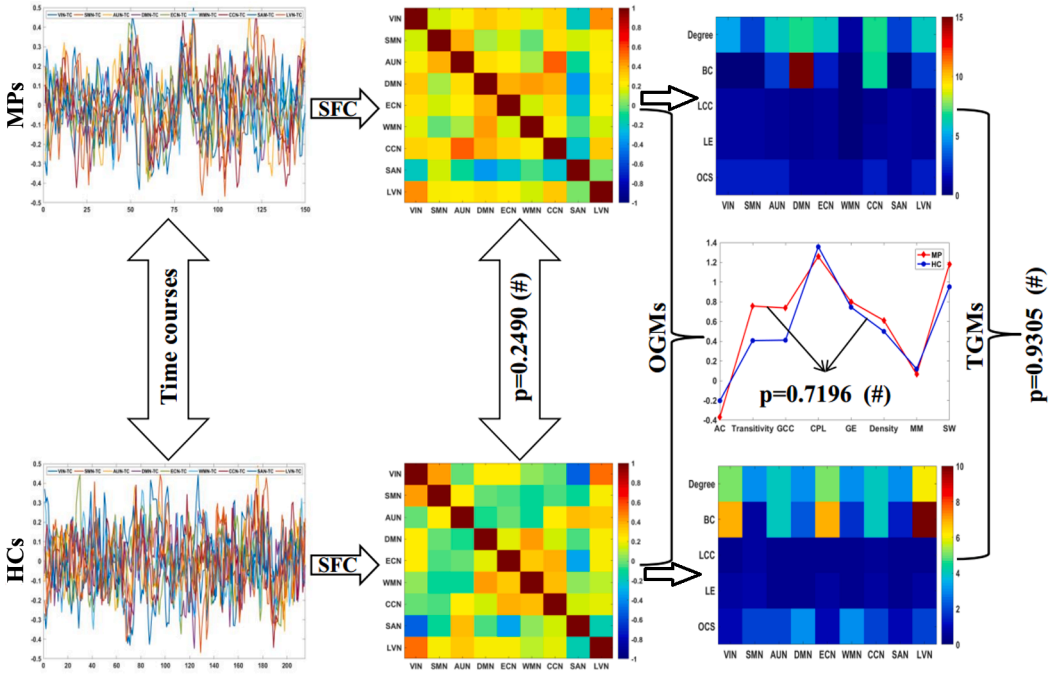

Fig. 2. the time courses of nine resting-state BFNs and the corresponding SFCs between them, as well as the comparison results of SFCs and their graph metrics between MPs and HCs at group level, including eight OGMs and five TGMs. Note: # denotes that there is no significant difference and * denotes that there is a significant difference between MPs and HCs.

Wilcoxon Rank sum test with a confidence level of 95% was used to statistically compare the difference between MPs and HCs on the variances of describing the dynamic variations of FCs and graph metrics in the DFCs analysis. All statistical results were corrected by false discovery rates (FDR), and these approaches had been used in the previous literature (Yu et al., 2015).

3. Results and analysis

In this section, we will present the results of MPs and HCs from both group and individual levels respectively, which obtained by the methods adopted in this study. Among them, we consider three window-width situations in DFCs analysis, including the situation of window-width of 40 s for both MPs and HCs, window-widths of 60 s and 40 s for MPs and HCs separately, as well as window-width of 60 s for both MPs and HCs. Meanwhile, eight one-dimensional graph metrics (OGMs) and five two-dimensional graph metrics (TGMs) are involved in the graph theory analysis among nine BFNs, including AC, Transitivity, GCC, CPL, GE, Density, MM and SM, as well as Degree, BC, LCC, LE and OCS. For the sake of brevity, we will not repeat them in the following paragraphs.

Fig. 1 shows the nine resting-state BFNs and their corresponding MNI coordinates for HCs and MPs, which obtained by using GICA at group level. These BFNs include visual networks (VIN), sensorimotor networks (SMN), auditory networks (AUN), default mode networks (DMN), executive control networks (ECN), working memory networks (WMN), cognitive control networks (CCN), salience networks (SAN) and lateral visual networks (LVN) respectively, which are obtained with threshold $|z| \geq 2$ after z-scored the ICs of GICA.

Table 1
the p-value and significance of each pair of DFCs and their whole variances between MPs and HCs under three window-widths at group level, which obtained by two-sample T-test and Wilcoxon rank sum test with a confidence level of 95% respectively.

	40 s/MPs,40 s/HCs	60 s/MPs,40 s/HCs	60 s/MPs,60 s/HCs
VIN vs SMN	3.15E−04(*)	1.71E−03(*)	4.08E−08(*)
VIN vs AUN	1.87E−06(*)	7.60E−09(*)	2.37E−14(*)
VIN vs DMN	7.65E−02	9.05E−02	7.85E−04(*)
VIN vs ECN	1.69E−03(*)	7.85E−03(*)	3.04E−06(*)
VIN vs WMN	1.03E−02(*)	4.61E−02(*)	1.47E−03(*)
VIN vs CCN	1.43E−03(*)	1.12E−06(*)	6.20E−11(*)
VIN vs SAN	4.33E−05(*)	2.67E−06(*)	4.79E−15(*)
VIN vs LAN	8.90E−10(*)	2.36E−08(*)	1.25E−09(*)
SMN vs AUN	2.85E−02(*)	4.88E−05(*)	3.77E−07(*)
SMN vs DMN	3.65E−03(*)	9.78E−05(*)	4.45E−05(*)
SMN vs ECN	2.30E−09(*)	1.75E−09(*)	2.65E−13(*)
SMN vs WMN	6.03E−05(*)	6.68E−06(*)	1.15E−06(*)
SMN vs CCN	1.05E−07(*)	6.53E−12(*)	1.01E−13(*)
SMN vs SAN	2.35E−02(*)	5.26E−03(*)	4.76E−06(*)
SMN vs LVN	4.60E−02(*)	4.85E−02(*)	1.31E−04(*)
AUN vs DMN	2.88E−12(*)	6.42E−16(*)	1.39E−17(*)
AUN vs ECN	8.94E−09(*)	6.65E−13(*)	1.45E−19(*)
AUN vs WMN	1.18E−13(*)	9.89E−19(*)	2.19E−17(*)
AUN vs CCN	1.65E−16(*)	9.17E−26(*)	2.50E−30(*)
AUN vs SAN	1.34E−33(*)	2.35E−33(*)	1.72E−46(*)
AUN vs LVN	7.78E−10(*)	1.62E−09(*)	9.58E−14(*)
DMN vs ECN	2.51E−02(*)	1.65E−04(*)	9.75E−08(*)
DMN vs WMN	2.90E−02(*)	4.98E−02(*)	2.06E−04(*)
DMN vs CCN	3.56E−02(*)	1.87E−03(*)	1.03E−06(*)
DMN vs SAN	1.20E−07(*)	7.16E−09(*)	1.92E−11(*)
DMN vs LVN	1.06E−01(*)	8.01E−03(*)	4.65E−04(*)
ECN vs WMN	5.45E−12(*)	1.96E−09(*)	8.30E−12(*)
ECN vs CCN	1.96E−03(*)	1.21E−02(*)	2.84E−05(*)
ECN vs SAN	2.01E−07(*)	4.62E−08(*)	1.28E−13(*)
ECN vs LVN	7.65E−03(*)	2.66E−02(*)	4.20E−04(*)
WMN vs CCN	6.99E−09(*)	4.84E−08(*)	1.87E−11(*)
WMN vs SAN	1.33E−01(*)	2.18E−02(*)	2.14E−05(*)
WMN vs LVN	1.54E−01(*)	3.26E−02(*)	4.55E−04(*)
CCN vs SAN	3.01E−10(*)	1.41E−11(*)	9.73E−16(*)
CCN vs LVN	8.30E−02	2.89E−03(*)	8.36E−06(*)
SAN vs LVN	9.60E−07(*)	1.77E−09(*)	1.49E−13(*)
DFC Variances	1.73E−04(*)	2.01E−01	8.40E−04(*)

Note: * denotes that there is a significant difference between MPs and HCs (the same in the below tables).

Fig. 2 shows the time courses of the above nine BFNs as well as SFCs between them for MPs and HCs at group level. Meanwhile, the comparison results of SFCs and their corresponding graph metrics between MPs and HCs are also presented, which obtained using two-sample T-test with a confidence level of 95% after FDR correction. Among them, SFCs and corresponding graph metrics are all compared on the whole among the nine BFNs between MPs and HCs, so that the degrees of freedoms are 70, 28 and 88 for SFCs, OGMs and TGMs respectively. It can be seen from the figure that there are no significant differences between the SFCs of MPs and those of HCs, which suggests that MPs have no obvious changes in the overall FCs among the nine BFNs compared with HCs.

In addition, the negative FCs between BFNs have been significant decreased in MPs compared with those in HCs, except for the FCs related to SAN, which may be due to the abnormal lateral brain activity in MPs. Meanwhile, we can also find that there are no significant differences in the OGMs and TGMs of SFCs between MPs and HCs, which indicates that the static topological properties of the nine BFNs in this study do not change significantly in MPs. Furthermore, it's worth noting that the OCS in all BFNs and all TGMs of SAN shown no obvious difference between MPs and HCs, which demonstrates that the influences of SAN on the topological structure of MP are limited, and OCS has little effect on characterizing the topological difference between MPs and HCs.

Table 1 shows the statistical p-values and significant differences between the DFCs of each pair of BFNs and overall DFC variances of MPs and HCs at group level under three window-width situations, where DFC variances are calculated by using all time-windows DFCs for each pair of BFNs. These comparison results are obtained by two-sample T-test and Wilcoxon rank sum test with a confidence level of 95% after FDR correction, where the degrees of freedoms are 332, 325 and 315 for the three window-width situations respectively.

Table 2
the p-value and significance obtained by two-sample T-test with a confidence level of 95% on the eight OGMs between MPs and HCs under three window-widths at group level.

Graph metrics	40 s/MPs,40 s/HCs	60 s/MPs,40 s/HCs	60 s/MPs,60 s/HCs
AC	3.20E−03(*)	1.11E−03(*)	4.51E−02(*)
Transitivity	7.29E−03(*)	7.62E−06(*)	1.30E−10(*)
GCC	2.29E−02(*)	2.59E−05(*)	2.11E−07(*)
CPL	7.21E−03(*)	2.79E−03(*)	2.09E−03(*)
GE	3.84E−03(*)	4.92E−04(*)	8.36E−05(*)
Density	1.99E−02(*)	9.25E−03(*)	6.33E−02
MM	3.86E−05(*)	2.80E−05(*)	5.54E−04(*)
SM	4.78E−03(*)	2.12E−03(*)	3.18E−02(*)

It can be seen from the table that there are significant differences in the DFCs of each pair of BFNs between MPs and HCs under three window-widths situations, except for a small amount of DFCs such as the DFCs of VIN vs DMN and CCN vs LVN in window-width of 40 s for both MPs and HCs, as well as the DFCs of VIN vs DMN in the window-widths of 60 s and 40 s for MPs and HCs separately. This suggests that the DFCs between BFNs have significant changes in MPs, and their connectivity strengths present a certain disturbance variation in different time periods.

Furthermore, the DFC variances among the nine BFNs show significant difference on the whole between MPs and HCs for two situations with the same window-widths except for the situation of window-widths of 60 s and 40 s for MP and HC separately. This suggests that MPs have obvious changes in the overall FCs among the nine BFNs compared with HC from the perspectives of the volatility of DFCs, and different window-widths have effects on describing this volatility.

Tables 2 and 3 show the statistical p-values and significant differences of the eight OGMs and five TGMs corresponding to DFCs between MPs and HCs at group level under three window-widths respectively, which obtained by two-sample T-test with a confidence level of 95% after FDR correction. All of these graph metrics are compared separately between MPs and HCs, where the degrees of freedoms are 332, 325 and 315 on all graph metrics for three window-width situations, respectively. It can be seen from the tables that all of OGMs have significant differences between MPs and HCs in the three window- widths situations, except for Density in the window-width of 60 s for both MPs and HCs. Meanwhile, most of TGMs have significant differences between MPs and HCs in the three window-widths, although there are still some TGMs showed no statistical difference between them. This suggests that the global topological properties among the nine BFNs in MPs have significant dynamic variation compared with those in HCs, while the variation of local topological properties in MPs presents some uncertainty compared with those in HCs. This may be due to the reason that the variation of local topological properties varies with different BFNs and different window-widths.

For instance, the OCS shows no obvious differences between MPs and HCs for most BFNs in the three window-widths, which may means that OCS has little effect on characterizing the topological difference between MPs and HCs. In addition to BC, the other four TGMs of SAN have significant difference between MPs and HCs in the window-width of 60 s for both MPs and HCs. But only LCC of SAN has a significant difference between MPs and HCs in the other two window-widths situations, which demonstrate that the influences of SAN on the topological structure among the BFNs are time-dependent in MPs. These results are consistent with the results in Fig. 2. However, the statistical analysis results of Fig. 2 and Tables 1–3 at group level ignore the individual differences of subjects in the group. Therefore, we further analyze the SFCs and DFCs

Table 3
The p-value and significance obtained by two-sample T-test with a confidence level of 95% on the five TGMs of each BFN between MPs and HCs under three window-widths at group level.

BFNs	Window-widths	Degree	BC	LCC	LE	OCS
VIN	40 s/MPs,40 s/HCs	1.57E−04(*)	3.60E−03(*)	1.13E−01	1.40E−01	1.05E−01
	60 s/MPs,40 s/HCs	1.35E−03(*)	7.84E−08(*)	2.72E−05(*)	3.23E−03(*)	7.75E−02
	60 s/MPs,60 s/HCs	3.21E−02(*)	1.15E−03(*)	2.22E−05(*)	3.73E−04(*)	3.81E−02(*)
SMN	40 s/MPs,40 s/HCs	6.66E−02	3.72E−03(*)	8.15E−03(*)	4.67E−03(*)	1.44E−01
	60 s/MPs,40 s/HCs	3.91E−02(*)	3.10E−04(*)	6.70E−08(*)	9.96E−08(*)	2.25E−01
	60 s/MPs,60 s/HCs	2.45E−03(*)	6.23E−03(*)	2.59E−07(*)	2.92E−08(*)	5.22E−02
AUN	40 s/MPs,40 s/HCs	4.85E−02(*)	6.07E−02	1.62E−01	1.46E−01	1.04E−01
	60 s/MPs,40 s/HCs	8.52E−08(*)	3.09E−04(*)	2.34E−02(*)	4.79E−03(*)	2.97E−01
	60 s/MPs,60 s/HCs	4.31E−06(*)	3.30E−03(*)	4.70E−06(*)	1.18E−05(*)	6.19E−02
DMN	40 s/MPs,40 s/HCs	4.40E−03(*)	3.26E−02(*)	1.34E−01	6.21E−02	7.78E−02
	60 s/MPs,40 s/HCs	7.12E−04(*)	1.01E−02(*)	8.08E−02	2.22E−02(*)	1.78E−01
	60 s/MPs,60 s/HCs	2.36E−08(*)	1.37E−06(*)	6.14E−02	1.10E−02(*)	2.68E−02(*)
ECN	40 s/MPs,40 s/HCs	3.73E−09(*)	3.20E−09(*)	1.34E−01	3.47E−02(*)	8.41E−03(*)
	60 s/MPs,40 s/HCs	3.74E−08(*)	9.37E−08(*)	1.79E−03(*)	9.61E−02	2.71E−01
	60 s/MPs,60 s/HCs	3.77E−12(*)	3.37E−09(*)	3.05E−06(*)	1.86E−03(*)	5.54E−03(*)
WMN	40 s/MPs,40 s/HCs	6.18E−02	4.40E−02(*)	8.87E−03(*)	9.07E−03(*)	6.29E−02
	60 s/MPs,40 s/HCs	4.64E−06(*)	9.78E−08(*)	1.94E−01	2.86E−01	1.55E−01
	60 s/MPs,60 s/HCs	6.46E−13(*)	1.03E−13(*)	2.57E−04(*)	1.74E−02(*)	6.24E−02
CCN	40 s/MPs,40 s/HCs	4.51E−08(*)	1.59E−02(*)	1.86E−02(*)	5.83E−03(*)	1.45E−01
	60 s/MPs,40 s/HCs	7.80E−08(*)	2.33E−02(*)	2.24E−03(*)	2.25E−04(*)	1.20E−01
	60 s/MPs,60 s/HCs	4.08E−10(*)	9.87E−04(*)	6.09E−03(*)	4.14E−04(*)	5.47E−02
SAN	40 s/MPs,40 s/HCs	1.44E−01	1.49E−01	2.92E−02(*)	7.19E−02	1.06E−01
	60 s/MPs,40 s/HCs	2.70E−01	2.99E−01	4.81E−02(*)	1.53E−01	1.24E−01
	60 s/MPs,60 s/HCs	1.73E−02(*)	5.33E−02	4.07E−04(*)	2.14E−03(*)	7.11E−03(*)
LVN	40 s/MPs,40 s/HCs	5.18E−02	1.78E−02(*)	1.30E−02(*)	2.63E−02(*)	1.44E−01
	60 s/MPs,40 s/HCs	8.06E−02	1.24E−01	5.27E−06(*)	1.28E−04(*)	1.31E−01
	60 s/MPs,60 s/HCs	5.06E−02	5.42E−02	3.61E−10(*)	2.38E−08(*)	1.20E−02(*)

of MPs and HCs at individual level, as shown in Fig. 3 and Tables 4–7.

Fig. 3 shows the time courses of above nine BFNs and the SFCs between them for all subjects of MPs and HCs at individual level, as well as the corresponding graph metrics included eight OGMs and five TGMs. Meanwhile, the comparison results of SFCs and graph metrics between MPs and HCs are also presented, which obtained by two-sample T-test with a confidence level of 95% and a degree of freedom of 95 after FDR correction. It can be seen from the figure that there are significant differences in the SFCs of each pair of BFNs between MPs and HCs, which suggests that the FCs of each pair of BFNs has changed in MPs compared with that in HCs. Similarity, the negative FCs between BFNs has been significantly decreased in MPs compared to HCs, which is consistent with the results in Fig. 2.

Furthermore, it can be seen from the figure that there are no significant differences in all OGMs of SFCs between MPs and HCs, which demonstrate that there are no significant changes in the global topology structure among BFNs across the whole time period in MPs compared with that in HCs. Meanwhile, most of the TGMs corresponding to SFCs also have no obvious differences between them, except for a few TGMs such as the Degree and BC of DMN, the LCC, LE and OCS of WMN, the Degree and LE of CCN, and the OCS of SAN, which suggests that these four brain networks play important roles in the change of local topology structure between BFNs in MPs. Moreover, the TGMs of Degree and BC in HCs are significantly higher than those in MPs.

Table 4 shows the statistical p-values and significant differences between the mean DFCs (MDFCs) and DFC variances (DFCVs) of each pair of BFNs for all subjects of MPs and HCs under three window-widths situations at individual level, which are obtained using two-sample T-test and Wilcoxon rank sum test with a confidence level of 95% and a degree of freedom of 95 after FDR correction, respectively. It can be seen from the table that there are significant differences in the MDFCs of most pairs of BFNs between MPs and HCs under three window-widths situations, except for a small amount of DFCs such as VIN vs WMN and VIN vs CCN et al. This suggests that the overall DFCs between nine BFNs have obvious changes in MPs compared with those in HCs, and has a high similarity among the three different window-width situations.

Meanwhile, the DFCs of subjects in each group exists obvious difference between different time-windows, which shows that the FCs between the nine BFNs is in a state of dynamic change during the entire period so that presents a different brain functional connectivity networks. In addition, we can find from the table that the DFCVs are significantly different in each pairs of BFNs between MPs and HCs in the situations of window-width of 40 s for both MP and HC and window-width of 60 s for both MPs and HCs, which indicates that the disturbance in different time periods has changes between them. However, only some DFCVs have significant differences between MPs and HCs in the window-widths of 60 s and 40 s for MPs and HCs separately, which may be due the reason that different window-widths are used in MPs and HCs, and this has a potential significance for studying the dynamic volatility of DFCs.

Table 5 shows the statistical p-values and significant differences between the mean OGMs (MOGMs) and OGMs variances (OGMVs) corresponding to DFCs in all subjects of MPs and HCs at individual level under three window-width situations, including AC, Transitivity, GCC, CPL, GE, Density, MM and SM. These comparison results are obtained by two-sample T-test and Wilcoxon rank sum test with a confidence level of 95% and a degree of freedom of 95 after FDR correction. It can be seen from the table that all of the MOGMs corresponding to DFCs have significant differences between MPs and HCs, indicating that the global dynamic topological properties among the nine BFNs have significant changed in MPs compared with those in HCs. Meanwhile, the DFCVs show significant differences between MPs and HCs in the situations of window-width of 40 s for both MPs and HCs as well as window-width of 60 s for both MPs and HCs except for the window-widths of 60 s and 40 s for MPs and HCs separately, which means that window-width has a significant influence in the volatility of DFCs dynamic changes.

Tables 6 and 7 show the statistical p-values and significant differences between the mean TGMs (MTGMs) and TGMs variances (TGMVs)

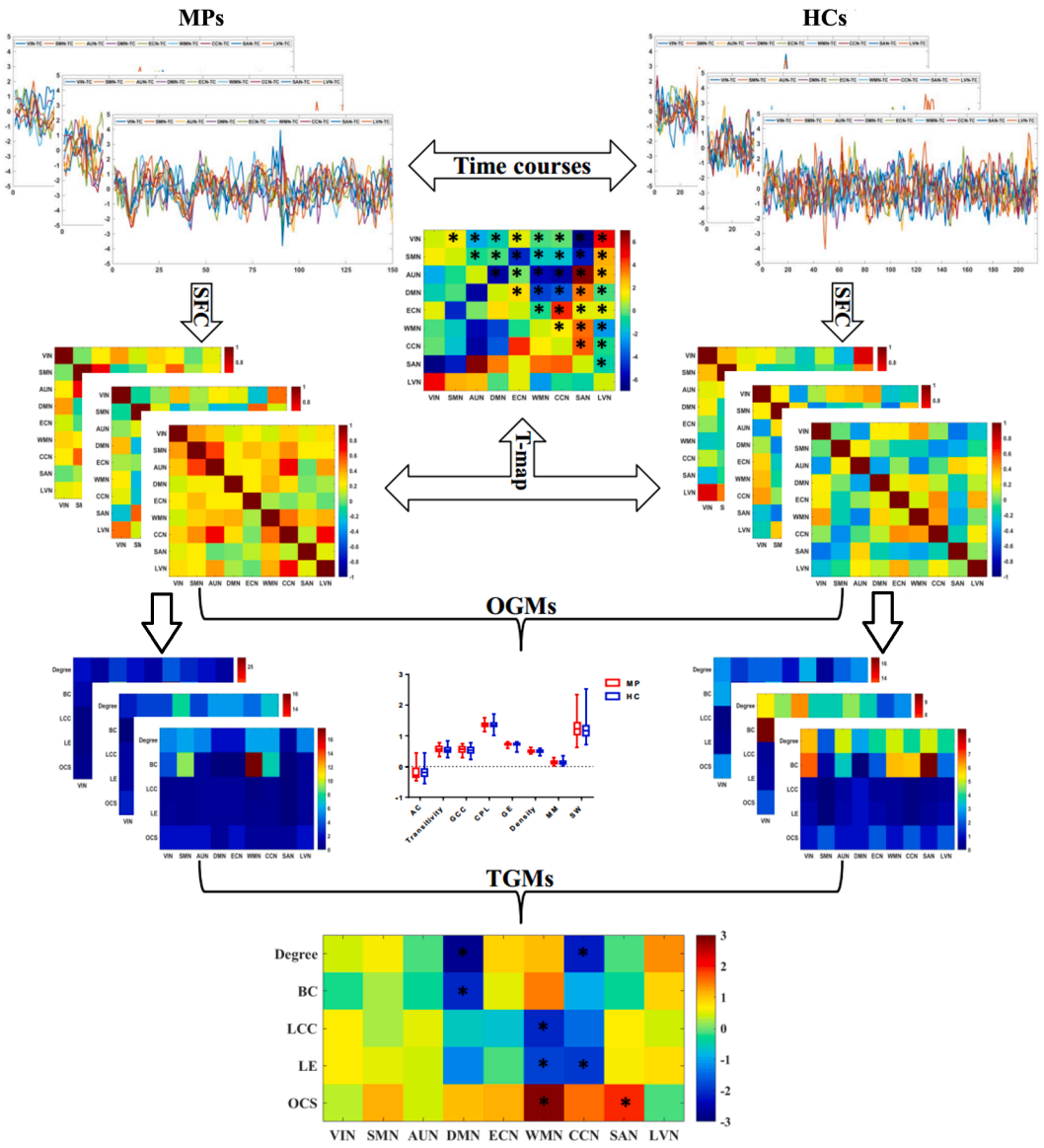

Fig. 3. the time courses of the nine resting-state BFNs at individual level and the SFCs between them, as well as the comparison results of SFCs and corresponding graph metrics between MPs and HCs. Note: * denotes that there is a significant difference between MPs and HCs.

corresponding to DFCs of all subjects in MPs and HCs at individual level under three window-widths situations respectively, including Degree, BC, LCC, LE and OCS. These comparison results are also obtained by two-sample T-test and Wilcoxon rank sum test with a confidence level of 95% and a degree of freedom of 95 after FDR correction.

It can be seen from Table 6 that the MTGMs of most BFNs corresponding to DFCs have no obvious differences between MPs and HCs in the three window-widths situations, except for a few TGMs of VIN, DMN, WMN and LVN. This suggests that these four BFNs play important roles in the change of local topology structure between BFNs in MPs. Moreover, they also show a certain degree of uncertainty in the situations of different window-widths, which means that different window-widths have effects on the local topological properties of the nine BFNs.

Meanwhile, the results in Table 7 demonstrate that the TGMVs are mainly significant different between MPs and HCs in the window-widths of 60 s and 40 s for MPs and HCs separately, while only a few MTGMs of BFNs are significantly different between MPs and HCs in other two window-width situations. This indicates that different window-widths have significant influences on the local topological variability of the nine BFNs between MPs and HCs.

Fig. 4 shows the DFC states obtained from the DFCs of subjects in MPs, the DFCs of subjects in HCs and the DFCs of all subjects in MPs&HCs in the three window-widths situations, including window-width of 40 s for both MPs and HCs, window-widths of 60 s and 40 s for MPs and HCs separately, as well as window-width of 60 s for both MPs and HCs, as shown (A)-(C). It can be seen from the figure that the number of DFC states obtained from three groups of DFCs under three window-width situations is 2, whether obtained from all DFCs of MPs&HCs or obtained from DFCs of MPs and HCs separately. However, the correlation between the DFC states obtained from different group of DFCs in the same window-width and the correlation between the DFC states obtained from the same group of DFCs in different window-widths cannot be observed obvious from the figure, which needs further quantitative analysis, as shown in Fig. 5.

Fig. 5 shows the correlation coefficients between DFC states obtained from the three groups of DFCs in Fig. 4 under three window-widths situations, as shown in (A). Meanwhile, the correlation coefficients between DFC states obtained from the same group of DFCs among the three window-widths are presented, as shown in (B). It can be seen from (A) in the figure that the two DFC states obtained from DFCs in MPs&HCs have

Table 4
the p-value and significance of MDFCs and DFCVs corresponding to each pair of BFNs between MPs and HCs under three window-widths at individual level, which obtained by two-sample T-test and Wilcoxon rank sum test with a confidence level of 95% after FDR correction, respectively.

FCs	40 s/MPs,40 s/HCs		60 s/MPs,40 s/HCs		60 s/MPs,60 s/HCs	
	MDFCs	DFCVs	MDFCs	DFCVs	MDFCs	DFCVs
VIN vs SMN	1.18E−01	4.40E−06(*)	1.23E−01	3.84E−02(*)	5.20E−02	8.99E−05(*)
VIN vs AUN	3.15E−03(*)	4.81E−06(*)	5.43E−03(*)	1.24E−01	1.96E−03(*)	8.82E−06(*)
VIN vs DMN	4.86E−02(*)	1.33E−08(*)	3.82E−02(*)	1.56E−01	2.57E−02(*)	4.49E−07(*)
VIN vs ECN	7.89E−03(*)	9.82E−08(*)	2.60E−02(*)	8.38E−02	6.55E−03(*)	1.61E−06(*)
VIN vs WMN	1.90E−01	3.94E−08(*)	1.62E−01	1.05E−01	6.74E−02	7.59E−06(*)
VIN vs CCN	1.85E−01	1.38E−05(*)	1.83E−01	4.85E−02(*)	6.77E−02	7.68E−05(*)
VIN vs SAN	1.47E−08(*)	3.17E−09(*)	2.16E−08(*)	1.15E−01	2.45E−09(*)	4.23E−07(*)
VIN vs LAN	2.89E−07(*)	4.35E−09(*)	1.07E−06(*)	4.66E−02(*)	6.96E−07(*)	4.10E−07(*)
SMN vs AUN	8.15E−02	6.31E−05(*)	4.63E−02(*)	7.57E−03(*)	3.35E−02(*)	7.79E−04(*)
SMN vs DMN	4.45E−02(*)	3.26E−09(*)	4.58E−02(*)	1.29E−01	2.75E−02(*)	3.87E−07(*)
SMN vs ECN	2.53E−09(*)	3.72E−09(*)	1.82E−08(*)	1.27E−01	3.16E−08(*)	2.35E−07(*)
SMN vs WMN	5.33E−03(*)	3.10E−09(*)	9.11E−03(*)	1.50E−01	3.64E−03(*)	3.71E−06(*)
SMN vs CCN	6.73E−03(*)	1.33E−05(*)	5.65E−03(*)	1.88E−02(*)	3.91E−03(*)	8.39E−04(*)
SMN vs SAN	1.83E−07(*)	4.44E−05(*)	2.20E−07(*)	1.15E−02(*)	1.41E−07(*)	8.24E−04(*)
SMN vs LVN	7.92E−03(*)	3.84E−07(*)	1.43E−02(*)	1.28E−01	3.45E−03(*)	5.11E−06(*)
AUN vs DMN	7.98E−09(*)	1.02E−07(*)	2.99E−08(*)	1.34E−01	1.32E−08(*)	1.37E−05(*)
AUN vs ECN	1.57E−01	1.24E−07(*)	1.98E−01	4.93E−02(*)	7.99E−02	1.40E−05(*)
AUN vs WMN	6.20E−09(*)	3.87E−08(*)	1.73E−08(*)	1.43E−01	2.18E−08(*)	1.44E−06(*)
AUN vs CCN	2.10E−07(*)	9.75E−05(*)	2.04E−08(*)	1.93E−02(*)	2.27E−08(*)	9.28E−04(*)
AUN vs SAN	3.02E−09(*)	1.34E−07(*)	1.14E−08(*)	1.52E−01	1.21E−09(*)	5.34E−06(*)
AUN vs LVN	5.97E−04(*)	1.80E−07(*)	4.36E−03(*)	1.39E−01	9.29E−04(*)	1.50E−06(*)
DMN vs ECN	2.88E−02(*)	6.40E−08(*)	5.14E−02(*)	1.28E−01	1.25E−02(*)	5.94E−07(*)
DMN vs WMN	7.26E−04(*)	4.06E−04(*)	1.34E−04(*)	3.70E−03(*)	7.94E−05(*)	3.03E−03(*)
DMN vs CCN	1.49E−04(*)	2.93E−06(*)	1.43E−04(*)	9.04E−03(*)	7.33E−05(*)	3.95E−04(*)
DMN vs SAN	9.27E−04(*)	1.78E−08(*)	3.06E−04(*)	4.50E−02(*)	6.85E−04(*)	1.95E−05(*)
DMN vs LVN	1.28E−01	1.59E−06(*)	1.02E−01	9.44E−02	5.10E−02	4.61E−05(*)
ECN vs WMN	1.17E−01	6.13E−06(*)	7.14E−02	4.72E−02(*)	3.35E−02(*)	7.52E−05(*)
ECN vs CCN	3.68E−05(*)	9.78E−09(*)	2.07E−05(*)	1.57E−01	8.12E−06(*)	1.37E−06(*)
ECN vs SAN	1.15E−01	7.43E−05(*)	6.97E−02	1.93E−02(*)	3.50E−02(*)	9.99E−04(*)
ECN vs LVN	1.55E−01	5.92E−07(*)	1.31E−01	1.53E−01	5.39E−02	1.36E−06(*)
WMN vs CCN	3.20E−02(*)	1.44E−08(*)	4.58E−02(*)	1.49E−01	1.23E−02(*)	1.43E−06(*)
WMN vs SAN	6.85E−04(*)	1.92E−09(*)	4.05E−04(*)	1.12E−01	3.20E−04(*)	8.14E−07(*)
WMN vs LVN	8.38E−04(*)	6.55E−07(*)	6.87E−04(*)	7.12E−02	7.20E−04(*)	4.07E−06(*)
CCN vs SAN	1.28E−04(*)	1.22E−06(*)	1.69E−04(*)	1.81E−02(*)	8.99E−05(*)	8.81E−05(*)
CCN vs LVN	7.34E−02	3.43E−05(*)	5.52E−02	2.06E−02(*)	3.09E−02(*)	4.00E−04(*)
SAN vs LVN	6.32E−02	9.49E−08(*)	6.36E−02	1.51E−01	3.29E−02(*)	6.05E−06(*)

Table 5
the p-value and significance of eight MOGMs and OGMVs corresponding to DFCs between MPs and HCs under three window-widths at individual level, which obtained by two-sample T-test and Wilcoxon rank sum test with a confidence level of 95% after FDR correction, respectively.

Graph metrics	40 s/MPs,40 s/HCs		60 s/MPs,40 s/HCs		60 s/MPs,60 s/HCs	
	MOGMs	OGMVs	MOGMs	OGMVs	MOGMs	OGMVs
AC	3.95E−05(*)	4.24E−03(*)	2.06E−03(*)	9.84E−01	2.02E−03(*)	4.54E−04(*)
Transitivity	5.49E−05(*)	3.81E−03(*)	1.28E−02(*)	5.71E−01	2.56E−03(*)	3.28E−04(*)
GCC	2.56E−04(*)	2.64E−03(*)	1.06E−02(*)	0.99E−01	4.44E−03(*)	7.22E−04(*)
CPL	2.18E−04(*)	3.04E−03(*)	4.82E−04(*)	6.16E−01	8.19E−03(*)	1.96E−04(*)
GE	8.32E−04(*)	4.51E−03(*)	1.02E−04(*)	4.98E−01	4.04E−03(*)	2.19E−04(*)
Density	4.59E−05(*)	3.02E−03(*)	2.21E−03(*)	8.61E−01	4.57E−03(*)	4.06E−04(*)
MM	4.33E−04(*)	3.55E−03(*)	1.53E−02(*)	0.99E−01	5.20E−03(*)	3.65E−04(*)
SM	4.36E−05(*)	3.24E−03(*)	2.32E−03(*)	5.22E−01	2.95E−03(*)	2.06E−04(*)

better correspondences with the two DFC states obtained from DFCs in MPs and HCs respectively in the three window-width situations. Among them, the correlation coefficient between one pair of DFC states is high, while the correlation coefficient between the other pair of DFC states is low.

This indicates that the two DFC states obtained from DFCs in MPs&HCs represent the commonality and differences between MPs and HCs, which can be further confirmed by the correspondence between the DFC states obtained from DFCs of MPs and HCs separately. Only one of these two states obtained from DFCs in MPs has a high correlation with another state obtained from DFCs in HCs in the three window-width situations, such as state 2 in MPs and state 1 in HCs, which indicates the potential specificity of DFCs in MPs compared with those in HCs. The state 1 in MPs presents the potentially unique DFC states in MPs, while state 2 in HCs reflects a normal functional connectivity between BFNs, and it changes significantly in MPs. In addition, the results in (B) show that the DFC states obtained from the same group of DFCs with different window-widths have good consistencies, which demonstrate the stability of FCs pattern reflected by the potential DFC states.

Fig. 6 shows the number of DFC states at individual level contained in each DFC state at group level obtained from the above three groups of DFCs in the three window-widths situations, as shown in (A). Meanwhile, the histograms of DFC states counts at individual level for MPs and HCs are presented in the three window-width situations, namely the number of subjects with a certain number of states identified, as shown in (B). It can be seen from (A) in the figure that the number of DFC states at individual level contained in these two DFC states at group level are close to each other for the above three cases of each window-width

Table 6
The p-value and significance obtained by two-sample T-test with a confidence level of 95% on the five MTGMs of each BFN between MPs and HCs under three window-widths at individual level.

BFNs	Window-widths	Degree	BC	LCC	LE	OCS
VIN	40 s/MPs,40 s/HCs	4.82E−01	5.00E−01	4.53E−02(*)	2.64E−02(*)	4.95E−01
	60 s/MPs,40 s/HCs	3.16E−02(*)	1.65E−01	3.02E−03(*)	2.78E−03(*)	1.11E−01
	60 s/MPs,60 s/HCs	5.15E−01	7.03E−01	1.27E−01	9.26E−02	1.55E−01
SMN	40 s/MPs,40 s/HCs	3.83E−01	4.31E−01	5.63E−01	5.95E−01	3.66E−01
	60 s/MPs,40 s/HCs	1.65E−01	1.76E−01	1.70E−01	1.50E−01	1.77E−01
	60 s/MPs,60 s/HCs	7.48E−01	7.39E−01	7.63E−01	7.24E−01	7.51E−01
AUN	40 s/MPs,40 s/HCs	5.68E−01	5.15E−02	3.82E−01	5.58E−01	3.13E−02(*)
	60 s/MPs,40 s/HCs	1.72E−01	1.47E−01	1.79E−01	1.80E−01	1.50E−01
	60 s/MPs,60 s/HCs	7.39E−01	2.42E−01	7.53E−01	7.78E−01	7.07E−01
DMN	40 s/MPs,40 s/HCs	1.36E−04(*)	7.28E−02	1.58E−03(*)	1.01E−03(*)	3.88E−01
	60 s/MPs,40 s/HCs	2.60E−03(*)	7.38E−03(*)	3.59E−02(*)	1.80E−02(*)	1.75E−01
	60 s/MPs,60 s/HCs	4.10E−03(*)	2.20E−02(*)	7.80E−02	3.89E−02(*)	7.52E−01
ECN	40 s/MPs,40 s/HCs	4.85E−01	1.89E−01	3.83E−01	5.86E−01	4.93E−01
	60 s/MPs,40 s/HCs	3.29E−02(*)	8.82E−02	1.49E−01	9.37E−02	1.79E−01
	60 s/MPs,60 s/HCs	5.31E−01	4.48E−01	7.39E−01	7.85E−01	7.22E−01
WMN	40 s/MPs,40 s/HCs	4.16E−01	7.20E−02	1.29E−03(*)	1.38E−02(*)	4.77E−02(*)
	60 s/MPs,40 s/HCs	1.81E−01	1.44E−01	2.17E−02(*)	4.06E−02(*)	9.75E−02
	60 s/MPs,60 s/HCs	5.58E−01	4.03E−01	7.02E−03(*)	2.38E−02(*)	5.56E−01
CCN	40 s/MPs,40 s/HCs	2.82E−02(*)	6.05E−01	2.94E−01	1.98E−01	3.21E−02(*)
	60 s/MPs,40 s/HCs	2.43E−02(*)	3.52E−02(*)	1.47E−01	1.82E−01	1.47E−01
	60 s/MPs,60 s/HCs	8.11E−02	5.04E−01	5.13E−01	3.42E−01	7.93E−01
SAN	40 s/MPs,40 s/HCs	3.76E−01	5.88E−01	3.99E−01	4.31E−01	4.62E−01
	60 s/MPs,40 s/HCs	6.21E−02	1.79E−01	9.27E−02	5.65E−02	1.28E−01
	60 s/MPs,60 s/HCs	7.17E−01	6.65E−01	7.46E−01	7.75E−01	5.57E−01
LVN	40 s/MPs,40 s/HCs	2.02E−01	3.16E−02(*)	5.80E−01	4.32E−01	3.33E−02(*)
	60 s/MPs,40 s/HCs	1.79E−02(*)	3.73E−02(*)	1.09E−01	5.56E−02	1.36E−01
	60 s/MPs,60 s/HCs	3.18E−01	5.36E−01	7.15E−01	5.34E−01	7.39E−01

Table 7
The p-value and significance obtained by Wilcoxon rank sum test with a confidence level of 95% on the five TGMVs of each BFN between MPs and HCs under three window-widths at individual level.

BFNs	Window-widths	Degree	BC	LCC	LE	OCS
VIN	40 s/MPs,40 s/HCs	8.21E−04(*)	1.27E−01	6.21E−02	2.55E−02(*)	3.13E−01
	60 s/MPs,40 s/HCs	8.18E−03(*)	2.46E−02(*)	9.89E−03	4.84E−03(*)	2.49E−02(*)
	60 s/MPs,60 s/HCs	1.05E−02(*)	6.97E−02	9.85E−02	6.80E−02	1.70E−01
SMN	40 s/MPs,40 s/HCs	3.25E−01	7.65E−02	3.39E−01	3.53E−01	2.07E−01
	60 s/MPs,40 s/HCs	7.36E−03(*)	3.70E−02(*)	3.91E−02(*)	3.69E−02(*)	2.61E−02(*)
	60 s/MPs,60 s/HCs	7.60E−02	3.87E−01	3.20E−01	3.01E−01	3.57E−01
AUN	40 s/MPs,40 s/HCs	2.84E−01	5.02E−02	2.03E−01	1.95E−01	8.21E−02
	60 s/MPs,40 s/HCs	1.73E−02(*)	1.05E−02	3.15E−02(*)	2.88E−02(*)	2.52E−02(*)
	60 s/MPs,60 s/HCs	1.90E−01	7.61E−02	1.52E−01	1.56E−01	1.80E−01
DMN	40 s/MPs,40 s/HCs	5.40E−02	2.77E−01	7.24E−03(*)	2.33E−03(*)	1.90E−01
	60 s/MPs,40 s/HCs	1.23E−03(*)	2.27E−02(*)	9.08E−04(*)	1.44E−03(*)	3.49E−02(*)
	60 s/MPs,60 s/HCs	1.59E−01	3.20E−02(*)	6.56E−02	3.00E−02(*)	1.89E−01
ECN	40 s/MPs,40 s/HCs	2.25E−01	2.58E−01	2.91E−01	2.54E−01	3.25E−01
	60 s/MPs,40 s/HCs	3.43E−02(*)	2.44E−02(*)	1.51E−02(*)	1.78E−02(*)	3.15E−02(*)
	60 s/MPs,60 s/HCs	5.79E−02	3.71E−01	8.45E−02	1.28E−01	3.63E−01
WMN	40 s/MPs,40 s/HCs	3.14E−01	2.59E−01	3.06E−01	2.15E−01	2.51E−02(*)
	60 s/MPs,40 s/HCs	3.07E−03(*)	2.51E−02(*)	2.62E−02(*)	2.29E−02(*)	3.08E−02(*)
	60 s/MPs,60 s/HCs	2.66E−01	1.74E−01	3.02E−01	1.75E−01	3.25E−01
CCN	40 s/MPs,40 s/HCs	3.19E−01	2.13E−01	2.08E−01	1.81E−01	3.07E−01
	60 s/MPs,40 s/HCs	8.94E−03(*)	3.76E−02(*)	9.52E−03(*)	1.43E−02(*)	1.71E−02(*)
	60 s/MPs,60 s/HCs	1.95E−01	1.70E−01	8.05E−02	8.58E−02	1.66E−01
SAN	40 s/MPs,40 s/HCs	2.12E−01	3.47E−01	3.06E−01	2.93E−01	3.14E−01
	60 s/MPs,40 s/HCs	2.56E−02(*)	2.86E−02(*)	1.77E−02(*)	1.50E−02(*)	3.68E−03(*)
	60 s/MPs,60 s/HCs	3.82E−02(*)	2.48E−01	1.38E−01	1.30E−01	1.68E−01
LVN	40 s/MPs,40 s/HCs	5.04E−02	1.71E−01	6.94E−02	7.20E−02	1.24E−01
	60 s/MPs,40 s/HCs	3.09E−02(*)	2.60E−02(*)	7.32E−03	6.86E−03(*)	3.21E−02(*)
	60 s/MPs,60 s/HCs	8.13E−02	1.58E−01	8.50E−02	7.45E−02	1.51E−01

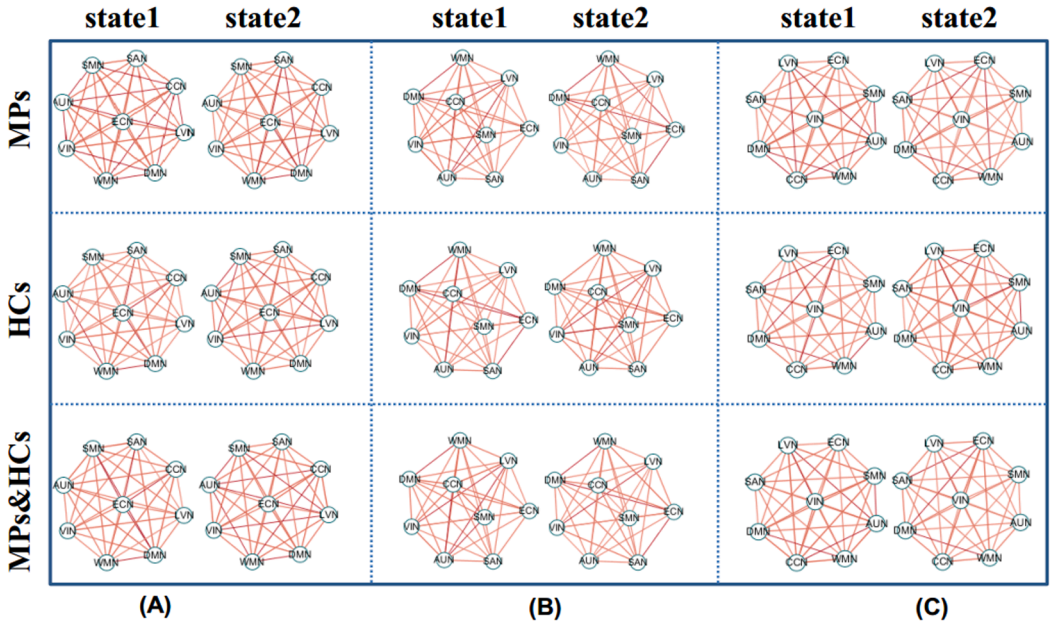

Fig. 4. The DFC states obtained from DFCs of all subjects in MPs&HCs, DFCs of subjects in MPs and DFCs of subjects in HCs under three window-widths of (A) 40 s for both MPs and HCs, (B) 60 s for MPs and 40 s for HCs, and (C) 60 s for both MPs and HCs.

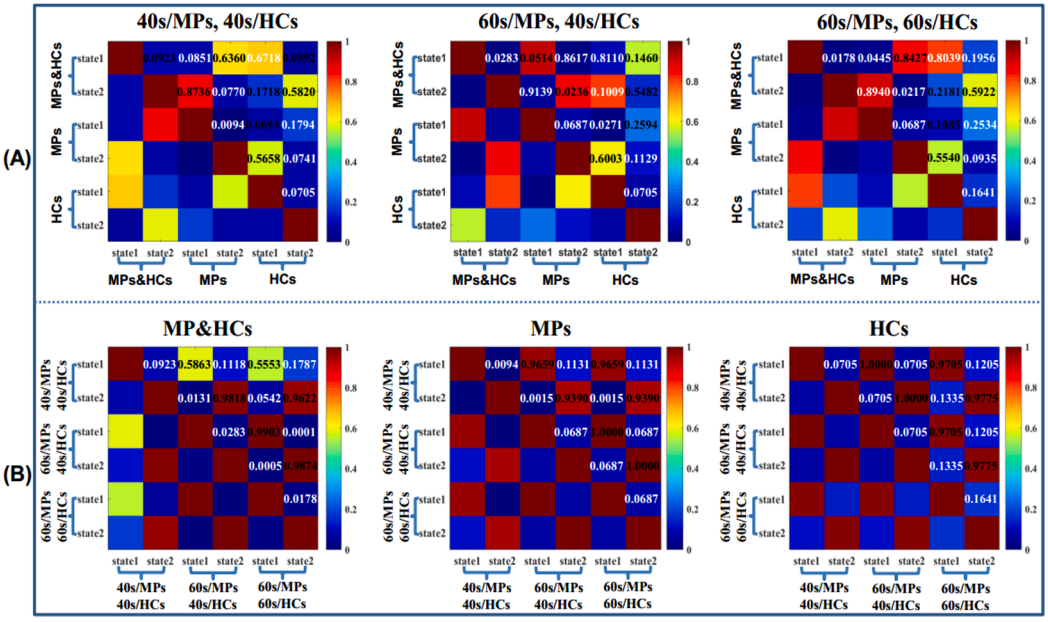

Fig. 5. **(A)** the correlation coefficients between DFC states obtained from three different groups of DFCs under three window-widths situations; (B) the correlation coefficients between DFC states obtained from the same group of DFCs among the three window-widths situations.

situation, which indicates the stability of these two states in the process of dynamic change for the above three cases and has highly reproducible for the DFC states of individual level in the three window-width situations. In addition, it can be seen from (B) in the figure that the number of DFC states with the most subjects obtained at individual level is 2 and 3 for MPs and HCs in the three window-widths situations, respectively.

Tables 8 and 9 shows the statistical p-values and significant differences of the OGMs and TGMs corresponding to the DFC states obtained from DFCs of all subjects in MPs and HCs under three window-width situations respectively, which obtained using two-sample T-test with a confidence level of 95% after FDR correction. The degrees of freedoms are 246, 259 and 265 on all graph metrics for three window-width situations, respectively. It can be seen from the tables that there are significant differences in the OGMs of these states between MPs and HCs in the three window-width situations, but only a few TGMs have significant differences between them, which suggests that the global topology properties among the nine BFNs of DFC states in MPs is significantly different from that in HCs, but the change of local topology properties is not obvious. Moreover, the corresponding TGMs differences between the DFC states of MPs and HCs under different window-widths are also different, which is consist with the results of DFCs at individual level.

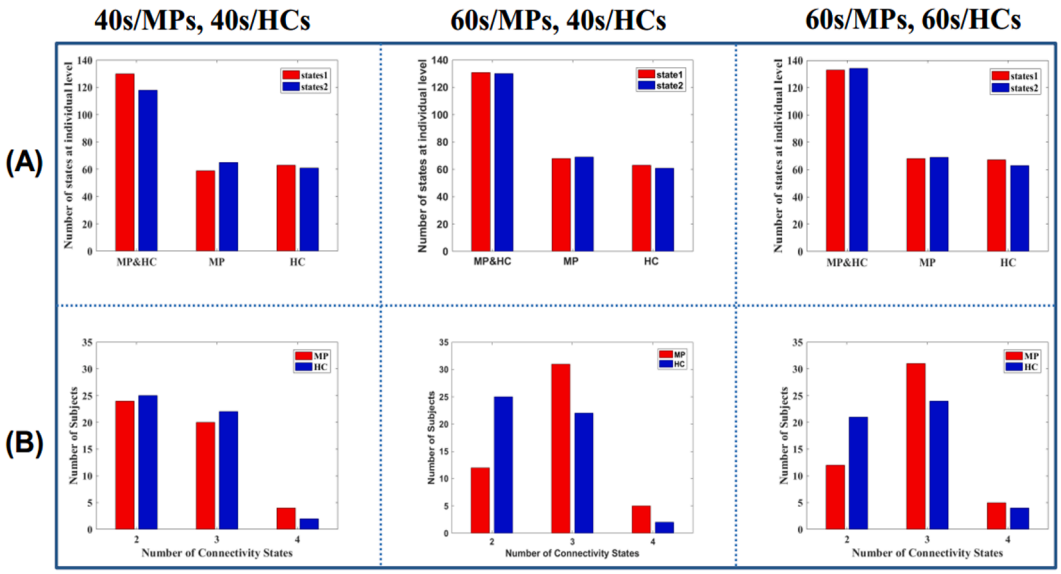

Fig. 6. (A) The number of DFC states at individual-level contained in each group DFC state of HC and MP groups under three window-widths; (B) Histogram of DFC states counts at individual level: Number of subjects with a certain number of state identified.

Table 8
the p-value and significance obtained by two-sample T-test with a confidence level of 95% on the eight OGMs of DFC states at individual level between MPs and HCs under three window-width situations.

Graph metrics	40 s/MPs,40 s/HCs	60 s/MPs,40 s/HCs	60 s/MPs,60 s/HCs
AC	1.66E−03(*)	4.96E−04(*)	5.41E−03(*)
Transitivity	1.24E−08(*)	4.97E−02(*)	1.90E−06(*)
GCC	6.35E−08(*)	1.37E−02(*)	3.93E−04(*)
CPL	5.85E−05(*)	3.67E−03(*)	5.36E−03(*)
GE	6.09E−04(*)	2.42E−04(*)	9.11E−03(*)
Density	2.88E−07(*)	3.92E−03(*)	6.95E−05(*)
MM	1.69E−04(*)	5.62E−02(*)	2.06E−05(*)
SM	1.08E−03(*)	3.47E−03(*)	1.20E−04(*)

4. Conclusion and discussion

The resting-state fMRI provides insights into pain circuits that are altered in migraine and could potentially contribute to the development of a new, noninvasive migraine biomarker. In this study, nine classical resting-state BFNs were obtained from fMRI data of MPs and HCs using GICA, and then the differences of these BFNs between MPs and HCs are systematically analyzed using multi-channel hierarchy, including SFCs and DFCs between these BFNs at group and individual levels, as well as their graph metrics and dynamic change characteristics of DFCs. The results demonstrated that there were significant differences on the FCs and their topology structure between the nine resting-state BFNs in MPs compared with those in HCs especially for the DFCs, which mean that the brain function activities have been obvious changed in MPs. The results may be provided a potential research perspective to reveal the pathogenesis of migraine and form a new biomarker.

Specifically, the results of Fig. 2 and Tables 1–3 at group level showed that there were no significant differences in the SFCs and corresponding static graph metrics among nine BFNs of MPs and HCs, while the DFCs and corresponding dynamic graph metrics between each pair of BFNs were significantly different in MPs compared with HCs. They demonstrated that the FCs and topological structure among these nine BFNs in MPs had a specific dynamic change in the whole time period at group level. However, it should be noted that TGMs with different BFNs have different effects under different window-widths, so there were uncertainty differences between MPs and HCs. In addition, different window-widths also have a certain influence on the change and fluctuation of DFCs.

Meanwhile, the results of Fig. 3 and Tables 4–7 at individual level showed that the SFCs and DFCs with their graph metrics between the nine BFNs had obvious difference in MPs compared with those in HCs, and the volatility of dynamic change and TGMs were influenced by the window-widths thus presenting some uncertainty. This was consistent with the results of group level in addition to SFCs, which may be due to the reasons for the differences between subjects. Furthermore, the results of Figs. 4–6 and Tables 8 and 9 demonstrated that the specificities of DFCs change patterns with corresponding topology structure and the consistency of DFC states under different window-widths in MPs among the nine BFNs involved in this study.

The sliding time-window technique is the most popular method for DFC analysis, but the choice of window length has always been a very controversial issue. On the one hand, too short window length increases the risk of introducing false fluctuations in the observed DFC (Hutchison et al., 2013; Zalesky and Breakspear, 2015), and also increases the risk of having too few samples to reliably calculate the correlation. On the other hand, too long a window can hinder the detection of the interest temporal variations. The previous study have showed that cognitive states could be correctly identified on 30–60 s of fMRI data (Shirer et al., 2012), and another study showed that changes of brain connectivity are not sensitive to the specific time-window length of 10–20 TRs (20–40 s) (Li et al., 2014).

Because the data of MPs and HCs used in this study comes from different sequences/scanners due to the reason that there is no data of HCs matching MPs available, which is indeed a shortcoming. Among them, the most likely is the effect of a different TR between MPs and HCs on the results of DFCs between BFNs. The same number of sliding windows of TRs make that MPs and HCs have different window-widths. Therefore, it needs to be further explored the influence of window-width on the analysis results of DFCs between BFNs in MPs and HCs. For this reason, the analysis results of DFCs under the situations of window-width of 40 s for both MPs and HCs, window-widths of 60 s and 40 s for MPs and HCs separately, as well as window-width of 60 s for both MPs and HCs were considered and compared in this study. The results showed that different window-widths have a certain influence on local topological properties and the volatility of dynamic changes, but little influence on FCs strength and global topological properties.

Prior studies showed that some highly structured, and quasi-stable connectivity patterns reoccurring over time could be assessed as a

Table 9
The p-value and significance obtained by two-sample T-test with a confidence level of 95% on the five TGMs of each BFN of the DFC states at individual level between MPs and HCs under three window-width situations.

BFNs	Window-widths	Degree	BC	LCC	LE	OCS
VIN	40 s/MPs,40 s/HCs	2.58E−01	8.65E−02	4.18E−01	7.75E−03	4.25E−01
	60 s/MPs,40 s/HCs	6.59E−02	9.59E−02	4.56E−02(*)	6.36E−02	3.90E−02(*)
	60 s/MPs,60 s/HCs	6.71E−01	6.00E−01	4.27E−01	7.49E−03	6.89E−01
SMN	40 s/MPs,40 s/HCs	3.71E−01	2.65E−02(*)	1.90E−01	3.20E−01	3.03E−01
	60 s/MPs,40 s/HCs	7.31E−02	5.06E−02	3.92E−02(*)	5.22E−02	9.12E−02
	60 s/MPs,60 s/HCs	1.64E−01	1.99E−02	4.70E−01	6.09E−01	6.52E−01
AUN	40 s/MPs,40 s/HCs	2.41E−01	7.82E−02	2.50E−01	6.25E−03	1.71E−01
	60 s/MPs,40 s/HCs	8.76E−02	9.25E−02	8.77E−02	8.65E−02	9.00E−02
	60 s/MPs,60 s/HCs	6.34E−01	4.73E−01	6.92E−01	4.10E−01	6.23E−01
DMN	40 s/MPs,40 s/HCs	4.25E−01	4.19E−01	2.40E−01	3.78E−01	2.59E−01
	60 s/MPs,40 s/HCs	7.99E−02	8.37E−02	3.90E−02(*)	1.02E−02	5.33E−02
	60 s/MPs,60 s/HCs	4.37E−01	1.92E−01	1.40E−01	3.19E−01	4.74E−01
ECN	40 s/MPs,40 s/HCs	1.85E−01	2.66E−02(*)	1.22E−03(*)	1.95E−01	1.62E−01
	60 s/MPs,40 s/HCs	5.12E−02	7.09E−02	9.15E−02	9.16E−02	7.18E−02
	60 s/MPs,60 s/HCs	5.56E−01	2.95E−01	5.54E−01	2.33E−02(*)	3.14E−01
WMN	40 s/MPs,40 s/HCs	1.48E−01	2.54E−01	3.79E−01	2.64E−01	2.51E−01
	60 s/MPs,40 s/HCs	9.06E−02	8.89E−02	1.86E−02(*)	6.23E−02	5.53E−02
	60 s/MPs,60 s/HCs	3.07E−01	2.83E−01	2.63E−01	4.19E−01	4.03E−01
CCN	40 s/MPs,40 s/HCs	3.17E−02(*)	1.89E−02(*)	2.63E−01	1.80E−01	1.81E−01
	60 s/MPs,40 s/HCs	7.27E−02	9.00E−02	8.98E−02	8.48E−02	9.39E−02
	60 s/MPs,60 s/HCs	2.50E−01	6.55E−01	8.18E−02	2.87E−01	4.10E−01
SAN	40 s/MPs,40 s/HCs	2.49E−01	1.80E−01	2.52E−01	5.87E−02	2.46E−01
	60 s/MPs,40 s/HCs	8.79E−02	9.16E−02	9.13E−02	8.46E−02	4.25E−02(*)
	60 s/MPs,60 s/HCs	3.48E−01	5.86E−01	6.62E−01	6.57E−01	2.73E−01
LVN	40 s/MPs,40 s/HCs	2.45E−01	2.22E−01	3.09E−01	4.44E−01	1.75E−01
	60 s/MPs,40 s/HCs	9.23E−02	4.01E−02(*)	6.05E−02	9.05E−02	8.98E−02
	60 s/MPs,60 s/HCs	4.97E−01	4.03E−01	6.38E−01	6.77E−01	2.72E−01

finite number of so called “connectivity states”, which reflect meaningful dynamic properties. Because the graph properties of the time-varying brain connectivity was considered in this study, a method based on graph metrics is used to explore the dynamic functional change rules between brain function networks, which could identify the connectivity patterns with similar graph organization that reoccurring over time (and subjects) and assemble them into connectivity states. Furthermore, it is different from the traditional clustering methods in the previous studies, which need to determine the number of classifications in advance. For example, Allen et al. estimated 7 connectivity states by using a k-means clustering method (Allen et al., 2014), while only two second-level connectivity state is established which shows the similar connectivity pattern as the stationary connectivity in this study, suggesting that the stationary connectivity pattern emerges most in the dynamic connectivity.

In addition, several classical resting brain functional networks are involved in this study, which have been reported in many researches. They are closely associated with basic cognitive functions in humans, as well as with the various cognitive and functional stimuli that trigger migraine symptoms. For example, DMN is closely related to personal introspection, memory, sensory information processing, thinking reasoning, emotional cognition, social reasoning and interpersonal communication. VIN and LVN are the basic and advanced visual networks, which play an important role in judging the basic features such as the size, shape, color and position of the object, and processes complex cognitive objects and can feedback the processed information to the original visual channel. AUN needs to coordinate the auditory networks, and SMN is involved in processing somatosensory information and planning movement tasks.

SAN involves in the process of attentional redirection induced by exogenous stimuli and is associated with both emotional and sensory stimulus drives. ECN and CCN are mainly related to cognitive stimulating activities, such as making plans, making decisions, judging right and wrong, responding to novel environments, and overcoming habitual actions. WMN is a cognitive system with a limited capacity that is responsible for temporarily holding information available for processing, which is important for reasoning and the guidance of decision-making and behavior. Therefore, the study on the FCs between these nine brain networks and their corresponding topological structure in this paper provides a promising perspective for exploring the neural pathogenesis of migraine patients, and also has certain a potential significance for the clinical diagnosis of migraine patients in the future.

Declaration of Competing Interest

All co-authors state that there is no conflict of interest.

Acknowledgments

This work was sponsored by Shanghai Sailing Program (Grant No. 19YF1419000), National Natural Science Foundation of China (Grants No. 61906117, 31870979), Pudong New Area Science and Technology Development Fund (Grant No. PKJ2014-Y08), and the Science and Technology Support Projects of the Shanghai Science and Technology Committee (Grant No. 19411971400).

References

Allen, E.A., Damaraju, E., Plis, S.M., Erhardt, E.B., Eichele, T., Calhoun, V.D., 2014. Tracking whole-brain connectivity dynamics in the resting state. Cereb. Cortex 24, 663–676.

Burstein, R., Noseda, R., Borsook, D., 2015. Migraine: multiple processes, complex pathophysiology. J. Neurosci. 35 (17), 6619–6629.

Calhoun, V.D., Adali, T., Pearlson, G.D., Pekar, J.J., 2001. A method for making group inferences from functional MRI data using independent component analysis. Hum. Brain Mapp. 14 (3), 140–151.

Cavina-Pratesi, C., Valyear, K.F., Culham, J.C., Kohler, S., Obhi, S.S., Marzi, C.A., Goodale, M.A., 2006. Dissociating arbitrary stimulus response mapping from movement planning during preparatory period: evidence from event-related functional magnetic resonance imaging. J. Neurosci. 26, 2704–2713.

De Luca, M., Smith, S., De Stefano, N., Federico, A., Matthews, P.M., 2005. Blood oxygenation level dependent contrast resting state networks are relevant to functional activity in the neocortical sensorimotor system. Exp. Brain Res. 167, 587–594.
Eck, J., Richter, M., Straube, T., Miltner, W.H.R., Weiss, T., 2011. Affective brain regions are activated during the processing of pain-related words in migraine patients. Pain 152, 1104–1113.
Fox, M.D., Raichle, M.E., 2007. Spontaneous fluctuations in brain activity observed with functional magnetic resonance imaging. Nat. Rev. Neurosci. 8, 700–711.
Greicius, M., 2008. Resting-state functional connectivity in neuropsychiatric disorders. Curr. Opin. Neurol. 24, 424–430.
Greicius, M.D., Srivastava, G., Reiss, A.L., Menon, V., 2004. Default-mode network activity distinguishes Alzheimer's disease from healthy aging: evidence from functional MRI. Proc. Natl. Acad. Sci. 101, 4637–4642.
Himberg, J., Hyvärinen, A., Esposito, F., 2004. Validating the independent components of neuroimaging time series via clustering and visualization. NeuroImage 22, 1214–1222.
Hutchison, R.M., Womelsdorf, T., Allen, E.A., Bandettini, P.A., Calhoun, V.D., Corbetta, M., Della Penna, S., Duyn, J.H., Glover, G.H., Gonzalez-Castillo, J., Handwerker, D.A., Keilholz, S., Kiviniemi, V., Leopold, D.A., de Pasquale, F., Sporns, O., Walter, M., Chang, C., 2013. Dynamic functional connectivity: promise, issues, and interpretations. NeuroImage 80, 360–378.
Jin, C., Yuan, K., Zhao, L., Zhao, L., Yu, D., von Deneen, K.M., Zhang, M., Qin, W., Sun, W., Tian, J., 2013. Structural and functional abnormalities in migraine patients without aura: brain abnormalities in migraine patients without aura. NMR Biomed. 26, 58–64.
Li, Y.-O., Adalı, T., Calhoun, V.D., 2007. Estimating the number of independent components for functional magnetic resonance imaging data. Hum. Brain Mapp. 28, 1251–1266.
Li, X., Zhu, D., Jiang, X.i., Jin, C., Zhang, X., Guo, L., Zhang, J., Hu, X., Li, L., Liu, T., 2014. Dynamic functional connectomics signatures for characterization and differentiation of PTSD patients: functional Connectomes. Hum. Brain Mapp. 35, 1761–1778.
Lui, S., Deng, W., Huang, X., Jiang, L., Ma, X., Chen, H., Zhang, T., Li, X., Li, D., Zou, L., 2009. Association of cerebral deficits with clinical symptoms in antipsychotic-naive first-episode schizophrenia: an optimized voxel-based morphometry and resting state functional connectivity study. AJP 166, 196–205.
Mainero, C., Boshyan, J., Hadjikhani, N., 2011. Altered functional magnetic resonance imaging resting-state connectivity in periaqueductal gray networks in migraine. Ann. Neurol. 70, 838–845.
Maleki, N., Gollub, R.L., 2016. What have we learned from brain functional connectivity studies in migraine headache? Headache: J. Head Face Pain 56 (3), 453–461.
Maleki, N., Linnman, C., Brawn, J., Burstein, R., Borsook, D., 2012. Her versus his migraine: multiple sex differences in brain function and structure. Brain 135, 2546–2559.
Mathur, V.A., Khan, S.A., Keaser, M.L., Hubbard, C.S., Goyal, M., Seminowicz, D.A., 2015. Altered cognition-related brain activity and interactions with acute pain in migraine. NeuroImage: Clin. 7, 347–358.
May, A., 2009. New insights into headache: an update on functional and structural imaging findings. Nat. Rev. Neurol. 5, 199–209.
Mickleborough, M.J.S., Ekstrand, C., Gould, L., Lorentz, E.J., Ellchuk, T., Babyn, P., Borowsky, R., 2016. Attentional network differences between migraineurs and non-migraine controls: fMRI evidence. Brain Topogr. 29, 419–428.
Moulton, E.A., Becerra, L., Maleki, N., Pendse, G., Tully, S., Hargreaves, R., Burstein, R., Borsook, D., 2011. Painful heat reveals hyperexcitability of the temporal pole in interictal and ictal migraine states. Cereb. Cortex 21, 435–448.
Newman, M.E.J., 2006. Modularity and community structure in networks. Proc. Natl. Acad. Sci. U.S.A. 103, 8577–8582.
Oshiro, Y., Quevedo, A.S., McHaffie, J.G., Kraft, R.A., Coghill, R.C., 2009. Brain mechanisms supporting discrimination of sensory features of pain: a new model. J. Neurosci. 29, 14924–14931.
Raichle, M.E., 2011. The restless brain. Brain Connect. 1, 3–12.
Rubinov, M., Sporns, O., 2010. Complex network measures of brain connectivity: uses and interpretations. NeuroImage 52, 1059–1069.
Russo, A., Tessitore, A., Esposito, F., Marcuccio, L., Giordano, A., Conforti, R., Truini, A., Paccone, A., d'Onofrio, F., Tedeschi, G., 2012a. Pain processing in patients with migraine: an event-related fMRI study during trigeminal nociceptive stimulation. J. Neurol. 259, 1903–1912.
Russo, A., Tessitore, A., Giordano, A., Corbo, D., Marcuccio, L., De Stefano, M., Salemi, F., Conforti, R., Esposito, F., Tedeschi, G., 2012b. Executive resting-state network connectivity in migraine without aura. Cephalalgia 32, 1041–1048.
Schwedt, T.J., Dodick, D.W., 2009. Advanced neuroimaging of migraine. Lancet Neurol. 8, 560–568.
Schwedt, T.J., Schlaggar, B.L., Mar, S., Nolan, T., Coalson, R.S., Nardos, B., Benzinger, T., Larson-Prior, L.J., 2013. Atypical resting-state functional connectivity of affective pain regions in chronic migraine. Headache: J. Head Face Pain 53 (5), 737–751.
Schwedt, T.J., Chong, C.D., Chiang, C.-C., Baxter, L., Schlaggar, B.L., Dodick, D.W., 2014. Enhanced pain-induced activity of pain-processing regions in a case-control study of episodic migraine. Cephalalgia 34, 947–958.
Schwedt, T.J., Chiang, C.-C., Chong, C.D., Dodick, D.W., 2015. Functional MRI of migraine. Lancet Neurol. 14, 81–91.
Seeley, W.W., Crawford, R.K., Zhou, J., Miller, B.L., Greicius, M.D., 2009. Neurodegenerative diseases target large-scale human brain networks. Neuron 62, 42–52.
Shi, Y., Zeng, W., Wang, N., Zhao, L.e., 2018. A new constrained spatiotemporal ICA method based on multi-objective optimization for fMRI data analysis. IEEE Trans. Neural Syst. Rehabil. Eng. 26, 1690–1699.
Shirer, W.R., Ryali, S., Rykhlevskaia, E., Menon, V., Greicius, M.D., 2012. Decoding subject-driven cognitive states with whole-brain connectivity patterns. Cereb. Cortex 22, 158–165.
Smith, S.M., Fox, P.T., Miller, K.L., Glahn, D.C., Fox, P.M., Mackay, C.E., Filippini, N., Watkins, K.E., Toro, R., Laird, A.R., Beckmann, C.F., 2009. Correspondence of the brain's functional architecture during activation and rest. Proc. Natl. Acad. Sci. U.S.A. 106, 13040–13045.
Tedeschi, G., Russo, A., Conte, F., Corbo, D., Caiazzo, G., Giordano, A., Conforti, R., Esposito, F., Tessitore, A., 2016. Increased interictal visual network connectivity in patients with migraine with aura. Cephalalgia 36, 139–147.
Tessitore, A., Russo, A., Giordano, A., Conte, F., Corbo, D., De Stefano, M., Cirillo, S., Cirillo, M., Esposito, F., Tedeschi, G., 2013. Disrupted default mode network connectivity in migraine without aura. J. Headache Pain 14.
Tessitore, A., Russo, A., Conte, F., Giordano, A., De Stefano, M., Lavorgna, L., Corbo, D., Caiazzo, G., Esposito, F., Tedeschi, G., 2015. Abnormal connectivity within executive resting-state network in migraine with aura. Headache: J. Head Face Pain 55, 794–805.
Wu, T., Wang, L., Chen, Y.i., Zhao, C., Li, K., Chan, P., 2009. Changes of functional connectivity of the motor network in the resting state in Parkinson's disease. Neurosci. Lett. 460, 6–10.
Yu, Q., Erhardt, E.B., Sui, J., Du, Y., He, H., Hjelm, D., Cetin, M.S., Rachakonda, S., Miller, R.L., Pearlson, G., Calhoun, V.D., 2015. Assessing dynamic brain graphs of time-varying connectivity in fMRI data: application to healthy controls and patients with schizophrenia. NeuroImage 107, 345–355.
Zalesky, A., Breakspear, M., 2015. Towards a statistical test for functional connectivity dynamics. NeuroImage 114, 466–470.
Zhang, J., Su, J., Wang, M., Zhao, Y., Zhang, Q.-T., Yao, Q., Lu, H., Zhang, H., Li, G.-F., Wu, Y.-L., Liu, Y.-S., Liu, F.-D., Zhuang, M.-T., Shi, Y.-H., Hou, T.-Y., Zhao, R., Qiao, Y., Li, J., Liu, J.-R., Du, X., 2017. The sensorimotor network dysfunction in migraineurs without aura: a resting-state fMRI study. J. Neurol. 264, 654–663.